ELSEVIER

# Effect of oxygen partial pressure on PLD cobalt oxide films

S. Laureti [a],*, E. Agostinelli [a], G. Scavia [a], G. Varvaro [a], V. Rossi Albertini [b],
A. Generosi [b], B. Paci [b], A. Mezzi [c], S. Kaciulis [c]

[a] ISM-CNR, P.O. Box 10, Area della Ricerca Roma1, Via Salaria km 29.300, 00016 Monterotondo Stazione, Roma, Italy
[b] ISM-CNR, Via Fosso del Cavaliere 100, 00100 Roma, Italy
[c] ISMN-CNR, P.O. Box 10, Via Salaria km 29.300 00016 Monterotondo Stazione, Roma, Italy

## Abstract

Thin CoO oxide layers with superior properties in terms of crystallographic ordering, surface roughness and constant and controlled chemical compositions have been prepared by pulsed laser deposition in reactive $O_2$ atmosphere at 400 °C. Such systems are particularly suitable both for applications and for basic studies, any time high quality and controlled surfaces are required, for example in multilayered systems whose behaviour critically depends on interface properties, such as magnetically exchange-coupled systems. A structural and microstructural study of such films is presented, together with the compositional analysis for different process conditions. The best control on film stoichiometry was obtained by protecting the surface with a thin Pt cap-layer, before air exposure.

## 1. Introduction

Recently, transition metal oxides have been studied for their optical, electrical, and magnetic properties, which can be used in a number of different applications [1,2]. Especially in advanced magnetic technology the coupling between an antiferromagnetic film, e.g. the CoO and NiO metal oxides, and a ferromagnetic layer (*exchange bias* systems), was proposed as an efficient tool to actually increase the functionality of magnetic nano-objects, by improving their properties as well as allowing their tuning to match specific applications. The *exchange bias* is an interfacial phenomenon strictly dependent on the thickness and the microstructure of the two involved nanometer thick layers [3]. The control of these properties during the fabrication process is an important tool for modifying the coupling. In this paper we present the study on cobalt oxide thin films ($d = 20$ nm) deposited by pulsed laser deposition by varying $O_2$ partial pressure. The main advantage

of using PLD over conventional deposition techniques is the higher average energy of deposited species that promote the growth of highly crystalline films with smoother surface also at low deposition temperatures. Moreover, many oxide systems have shown improved properties if deposited by laser ablation: this is the case of the well known high-$T_c$ superconductors [4] or $Co_3O_4$ as anode material in lithium ion batteries [5] or CoO as gas sensor [6].

The structural and microstructural properties were studied by X-ray diffraction (in energy dispersive mode) and AFM analysis, while the chemical composition of the samples was investigated by using X-ray photoelectron spectroscopy (XPS).

## 2. Experimental

Cobalt oxide films were deposited on Si (1 0 0) substrates at a growth temperature of 400 °C in a high vacuum PLD chamber. Depositions were performed by focusing a pulsed KrF Lambda Physik excimer laser ($\lambda = 248$ nm, pulse duration = 17 ns) on a rotating Co target. The spot energy fluence was 3 J/cm$^2$, and the pulse repetition rate was 1 Hz for a total of 7200 pulses. Substrate and target were assembled in a frontal

\* Corresponding author. Tel.: +39 0690672651; fax: +39 0690672316.
E-mail address: sara.laureti@ism.cnr.it (S. Laureti).

geometry at 50 mm reciprocal distance. The PLD chamber was evacuated up to a base pressure of $1 \times 10^{-6}$ mbar prior to the film deposition. The oxide growth was obtained in a reactive atmosphere produced by an $O_2$ dynamic gas flow through a needle valve. A series of samples was grown at different $O_2$ pressure ranging from $10^{-4}$ up to $10^{-2}$ mbar.

The energy dispersive X-ray diffraction (EDXD) technique was used for the structural characterization of the films. It is an unconventional method particularly suitable when a fast diffraction pattern collection and rocking curve (RC) analysis of various samples are required. The basic theoretical principles ruling the EDXD technique are reported in [7].

In the ED mode, the X-ray diffraction patterns are collected using a X-ray polychromatic beam, at a fixed scattering angle $2\theta$ via a solid state detector capable to detect both the number and the energy of the photons diffracted by the sample.

The RC of a polycrystal represents the weighted statistical distribution of the crystallites orientation. Defining the asymmetry parameter $\alpha$ as $(\theta_i - \theta_r)/2$, where $\theta_i$ is the primary beam incidence angle with respect to the film surface and $\theta_r$ is the reflection angle, the RC is obtained by normalizing the intensity of a given Bragg peak, as a function of $\alpha$ (while the total scattering angle $(\theta_i + \theta_r) = 2\theta$ is kept unchanged), to its maximum intensity detected along the $\alpha$-scan.

When RC measurements are performed, the ED mode is particularly convenient, since all Bragg peaks present in the selected region of the scattering parameter are collected simultaneously.

A non-commercial apparatus was used for ED diffractometry [8]. The diffraction measurements were performed upon the set of CoO/Si films in the same experimental conditions allowing to work in the 15–55 keV X-ray energy range, keeping the scattering angle fixed at $2\theta = 14.00°$. The setup was kept unchanged during the rocking curve data collection ($\alpha$-scan), the $\alpha$ variation range being $-0.1° < \alpha < 0.1°$.

Photoemission spectra were collected by a VG ESCALAB MkII spectrometer, equipped with a standard X-ray excitation source of Al K$\alpha$ (1486.6 eV) and a 5-channeltron detection system. The measurements have been performed at a pressure of about $1 \times 10^{-10}$ mbar, that has been increased up to $1 \times 10^{-7}$ mbar during the depth profiling. The energy of the ion gun (Ar$^+$) has been set at 2.0 keV and the sample current density to $2 \times 10^{-3}$ mA cm$^{-2}$, which corresponds to the average sputtering rate of about 0.2 nm min$^{-1}$ [9]. The binding energy (BE) scale was calibrated by measuring the C 1s peak (BE = 285.0 eV) from the surface contamination. The accuracy of the BE values was $\pm 0.1$ eV.

The scanning probe microscopy (SPM) measurements were made by using a home-made atomic force microscope operating both in contact and in non-contact mode.

## 3. Results and discussion

The chemical composition of the films was investigated by XPS. The spectra of the main photoelectron lines (Co 2p, O 1s and Si 2p) were acquired and processed by standard XPS peak-fitting routine. In Fig. 1 are shown typical Co 2p spectra for the
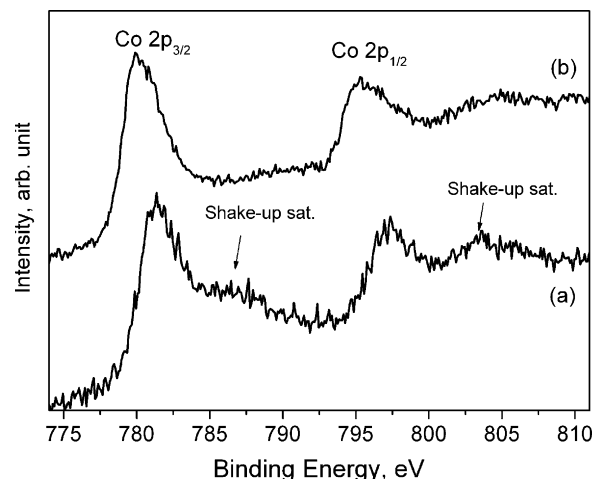


Fig. 1. Co 2p spectrum of (a) CoO and (b) $Co_3O_4$.

CoO and $Co_3O_4$, characterized by a spin-orbit doublet $2p_{3/2}$ and $2p_{1/2}$ separated in energy by 15.4 eV. As it is known from the literature [10–12], a strong peak of Co $2p_{3/2}$ at 778.2 eV is characteristic for Co$^0$, while two peaks of different oxides are located at 780.1 and at 781.3 eV for $Co_3O_4$ and CoO, respectively. Moreover, the Co 2p spectrum of the CoO is characterized by the presence of strong peaks of shake-up satellites positioned at $\sim$6 eV above the main peaks Co $2p_{3/2}$ and Co $2p_{1/2}$, (see the spectrum (a) in Fig. 1). The presence of shake-up satellites is due to the paramagnetic and high-spin Co(II) electronic configuration in the CoO oxide, while these satellites are not present in Co 2p spectrum of normally diamagnetic and low-spin Co(III) in $Co_2O_3$. Since $Co_3O_4$ is a combination of the two oxides CoO and $Co_2O_3$, its spectrum will be described by the combination of the contributions of these two oxides with a ratio Co(II):Co(III) = 1:2. Therefore, the intensity of shake-up satellites in Co 2p spectrum of $Co_3O_4$ is expected to be low, as it is in the spectrum (b) in Fig. 1. More detailed interpretation of XPS spectra of cobalt oxides has been reported in Ref. [13].

In this work, samples deposited at increasing $O_2$ pressure ($10^{-4}$, $10^{-3}$ and $10^{-2}$ mbar) were analyzed. The XPS depth profiling revealed that films grown at the lowest $O_2$ pressure are composed predominantly of metallic cobalt. Below a thin CoO surface layer (less than 1 nm), films are only partially oxidized with a dominant contribution of metallic Co at BE = 778.2 eV (see Co $2p_{3/2}$ spectrum in Fig. 2) and the oxide contribution is disappearing going towards the Co/Si interface. This was confirmed by EDXD investigation. Indeed, the diffraction pattern relative to samples deposited at an $O_2$ pressure of $10^{-4}$ mbar (Fig. 3), shows that only three crystalline Bragg peaks are present, which can be attributed to metallic Co: the [1 0 0] reflection at $q = 2.88(1)$ Å$^{-1}$, the [1 1 1] reflection at $q = 3.07(1)$ Å$^{-1}$, and the [1 0 1] reflection at $q = 3.27(1)$ Å$^{-1}$. Moreover, the [2 0 0] and [4 0 0] contributions of the Si substrate (at $q = 2.320(5)$ Å$^{-1}$ and at $q = 4.630(5)$ Å$^{-1}$, respectively) are also visible. Spurious signals arising from the Ag paste used to hold the substrate on the substrate holder were also occasionally detected. Indeed, as visible in Fig. 3, the Ag fluorescence lines and the [1 1 1] and [2 2 0] reflections at $q = 2.66(1)$ Å$^{-1}$ and at $q = 4.35(1)$ Å$^{-1}$ are also present.
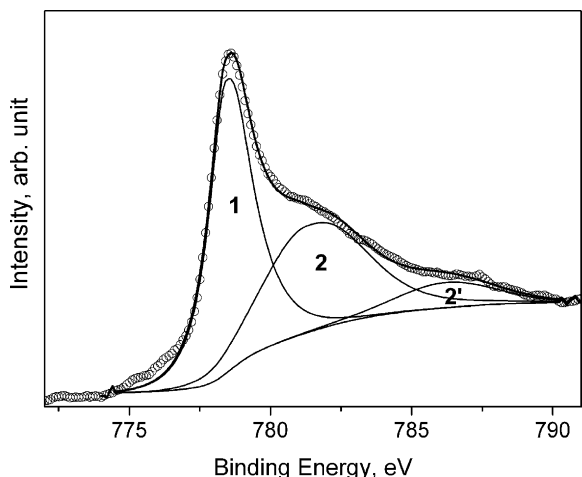
Fig. 2. XPS curve-fitting of the Co $2p_{3/2}$ peak of the sample deposited with an $O_2$ pressure of $10^{-4}$ mbar: 1-$Co^0$ (778.4 eV); 2-CoO (781.3 eV); $2'$-shake-up satellite of the Co $2p_{3/2}$ main peak of CoO.



Fig. 4. Diffraction pattern relative to the sample deposited at an $O_2$ pressure of $1 \times 10^{-3}$ mbar: no pure Co reflections are visible, while the [3 1 1] reflection at $q = 4.90$ Å$^{-1}$ is the contribution of the CoO cubic phase.

When $O_2$ pressure was increased up to $1 \times 10^{-3}$ mbar, the surface composition was characterized by a $Co_3O_4$ thin layer. Below such layer, a CoO uniform composition was observed down to the Si interface, where a weak contribution from metallic Co was still evidenced. The EDXD pattern of this sample showed the absence of pure Co reflections, while the contribution of the CoO cubic phase, the [3 1 1] reflection at $q = 4.90$ Å$^{-1}$, became visible (Fig. 4).

Increasing $O_2$ pressure up to at $10^{-2}$ mbar produced a further Co oxidation and the increasing of $Co_3O_4$ oxide concentration; this can be seen by EDXD results reported in Fig. 5, where $Co_3O_4$ was the main oxide evidenced. The [2 2 2] reflection at $q = 2.66(1)$ Å$^{-1}$, the [4 0 0] reflection at $q = 3.06(1)$ Å$^{-1}$, the [5 3 3] reflection at $q = 5.07(1)$ Å$^{-1}$ and the [4 4 4] reflection at $q$ 5.32(1) Å$^{-1}$ were all attributed to the $Co_3O_4$ polycrystalline

phase. The peak at $q = 4.20(1)$ Å$^{-1}$ attributed to the CoO oxide [2 2 0] reflection, showed a negligible intensity.

XPS analysis revealed that $Co_3O_4$ is present on the sample surface. After only few minutes of ion sputtering, the shape of the Co 2p signal changed indicating the dominant contribution of CoO. The quantitative XPS depth profile of this sample is presented in Fig. 6. Some traces of surface contamination with carbon (not shown in the profile) were completely removed rapidly after few cycles of sputtering. The volume of the film was composed of pure and uniform CoO film with estimated total thickness of about 15 nm. However, the ratio O:Co in this film was slightly lower than the stoichiometric value 1, probably due to the preferential ion sputtering which can cause a partial reduction of oxide [13,15]. Near the film/substrate interface, a component at BE = 778.7 eV appeared in the Co 2p spectrum.
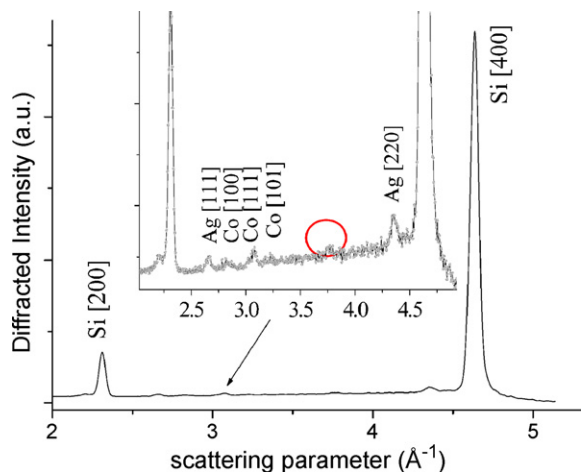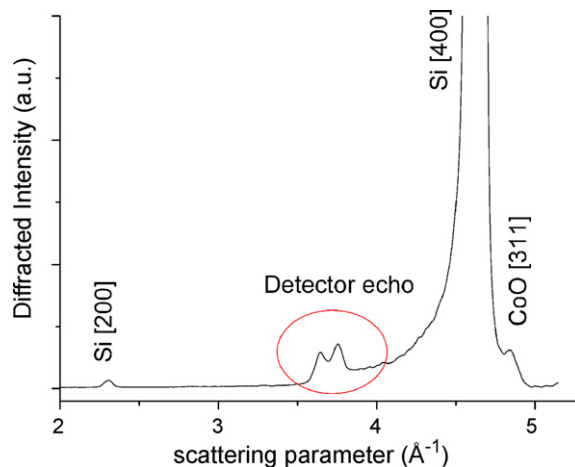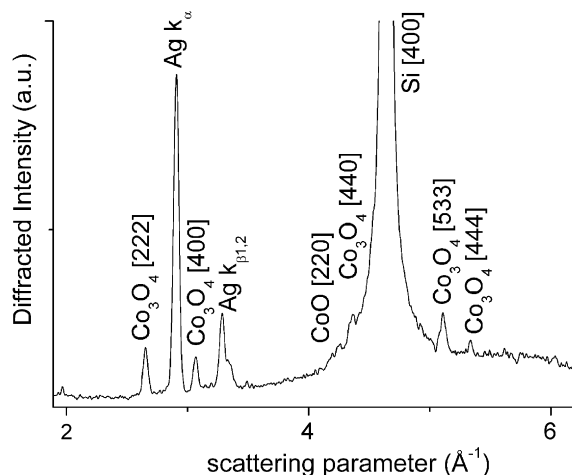


Fig. 3. Diffraction pattern relative to the sample deposited at an $O_2$ pressure of $10^{-4}$ mbar: the Co [1 0 0] reflection at $q = 2.88(1)$ Å$^{-1}$, the Co [1 1 1] reflection at $q = 3.07(1)$ Å$^{-1}$, and the Co [1 0 1] reflection at $q = 3.27(1)$ Å$^{-1}$ are visible. The Si [2 0 0] and [4 0 0] contributions, at $q = 2.320(5)$ Å$^{-1}$ and at $q = 4.630(5)$ Å$^{-1}$, respectively, are also visible. The Ag fluorescence lines and the Ag [1 1 1] and Ag [2 2 0] reflections, at $q = 2.66(1)$ Å$^{-1}$ and at $q = 4.35(1)$ Å$^{-1}$, arising from the Ag paste, are also present.



Fig. 5. Diffraction pattern relative to the sample deposited at an $O_2$ pressure of $10^{-2}$ mbar: the [2 2 2] reflection at $q = 2.66(1)$ Å$^{-1}$, the [4 0 0] reflection at $q = 3.06(1)$ Å$^{-1}$, the [5 3 3] reflection at $q = 5.07(1)$ Å$^{-1}$ and the [4 4 4] reflection at $q$ 5.32(1) Å$^{-1}$ are all attributed to $Co_3O_4$ polycrystalline phase. The peak at $q = 4.20(1)$ Å$^{-1}$ is attributed to CoO oxide [2 2 0] reflection, showing a negligible intensity.
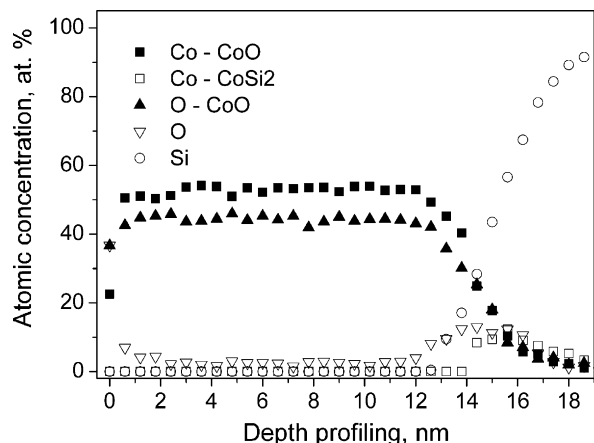
Fig. 6. XPS depth profile of the sample D.



Fig. 8. XPS depth profile of the sample C.

This value is slightly higher then the BE of Co(0) and it is closer to the value of $CoSi_2$ [14]. Since the contribution of metallic cobalt was increasing with increasing Si signal (99.2 eV), we suppose that metallic cobalt was embedded into Si substrate during the first stage of film deposition. When Co and Si are in direct contact, a silicide compound ($CoSi_2$) can be formed. From the depth profile, the intermixing sublayer of Co and Si was estimated to be about 4 nm thick. Finally, the presence of $SiO_2$ at the film/substrate interface is due to the native oxide on the substrate that was not eliminated before the deposition.

The comparison of the results obtained at increasing $O_2$ pressure indicates that two oxidation processes were taking place during the film growth. The direct oxidation during film deposition was observed only for $O_2$ pressure higher than $1 \times 10^{-3}$ mbar. On the other hand, a surface oxidation always occurred after the film deposition, as it was evidenced by XPS analysis showing higher oxidation state on the surface. As a matter of fact, we have observed that the films, grown at a higher $O_2$ pressure, were characterized by increasing contribution of $Co_3O_4$ oxide, probably because the hot film surface after the deposition was exposed to the enriched $O_2$ atmosphere before recovering the vacuum in the deposition chamber. In such a way the newly formed $Co_3O_4$ layer showed also an improved crystallinity and some long range order, as it was evidenced by higher intensity of the $Co_3O_4$ reflections in EDXD diffraction pattern.
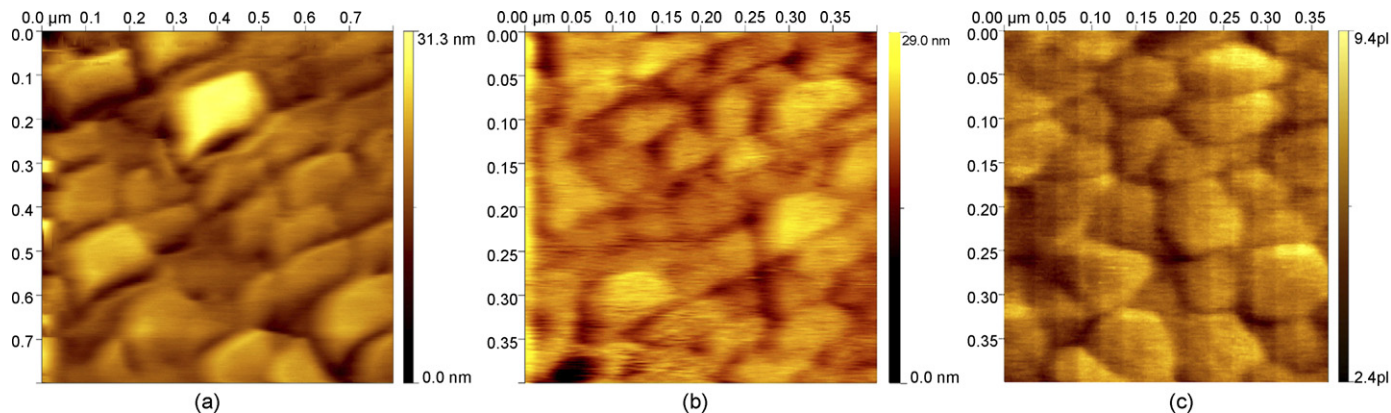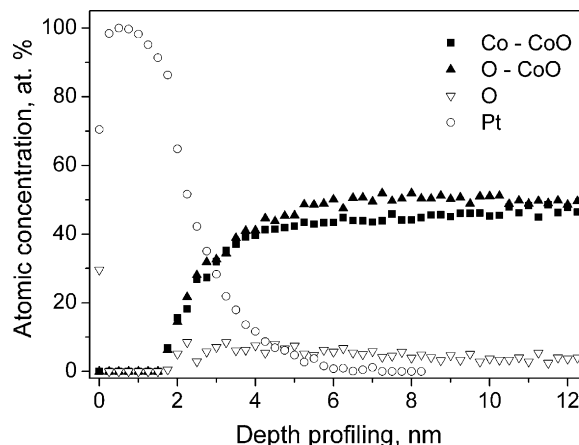
The film morphology variations with increasing $O_2$ pressure was investigated (Fig. 7). The surface of films deposited at the lowest pressure consisted of a homogeneous distribution of crystallites with rectangular shape and dimensions ranging from 100 to 150 nm (mean square roughness Rms = 3.5 nm). These structures were attributed to superficial CoO as shown by XPS. By increasing $O_2$ pressure, the surface was characterized by a prevalence of faceted crystallites probably due to the $Co_3O_4$ phase, with dimensions ranging from 50 to 80 nm, even if regions with more rectangular crystallites attributable to CoO were still present. The surface roughness did not sensibly change (Rms = 3.3 nm). In samples grown at $10^{-2}$ mbar, faceted $Co_3O_4$ crystallites with bigger dimension (ranging from 80 to 100 nm) and with a more defined crystalline habit were observed. $Co_3O_4$ films with crystallite morphology very similar to our samples were also reported in [5].

We can conclude that, in order to obtain a pure CoO film with homogeneous composition, an oxygen pressure of $10^{-3}$ mbar has to be used and the film surface has to be protected to avoid the oxidation process to go on further with $Co_3O_4$ formation. For this purpose, a thin Pt overlayer (about 2 nm thick) was deposited immediately after CoO deposition. Such samples showed a very uniform CoO composition, starting from the oxide surface after the removal of protective overlayer of Pt down to the substrate, as it can be seen in the depth profile shown in Fig. 8.
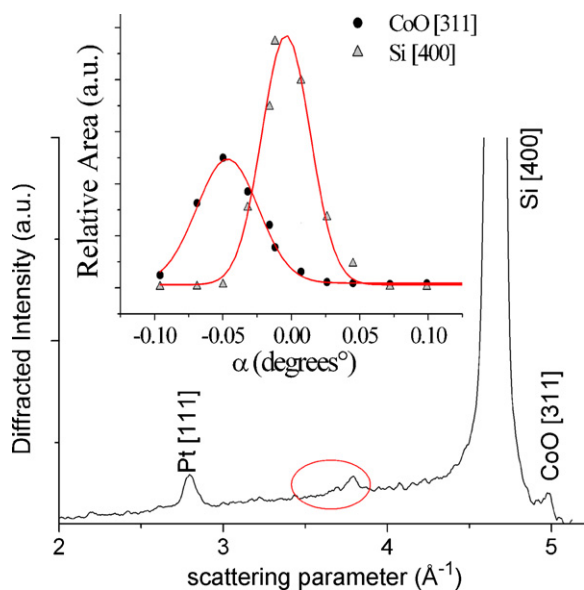


Fig. 7. AFM images of samples grown at $10^{-4}$ (a), $10^{-3}$ (b) and $10^{-2}$ (c) mbar.

Fig. 9. Diffraction pattern relative to the sample covered by the Pt cap-layer: the Pt [1 1 1] reflection is visible at $q = 2.88(1)$ Å$^{-1}$. The insert shows the result of the rocking curve analysis of the CoO [3 1 1] reflection, compared to the Si [4 0 0] reflection from the substrate.

A detailed structural characterization of such samples was obtained by ED diffraction and the RC analysis was performed in order to obtain more accurate information about the internal order of the crystalline phases, i.e. the degree of epitaxy of the textured film. The CoO film was grown as a pure [3 1 1] crystalline phase (Fig. 9). The other Bragg peaks were assigned to the [4 0 0] Si reflection contribution from the substrate and to Pt [1 1 1] cap-layer at $q = 2.88(1)$ Å$^{-1}$. As discussed above, the rocking curve analysis of the CoO [311] reflection was performed collecting diffraction patterns at different $\alpha$ values, and the results are shown in the inset of Fig. 9. The CoO film turned out to be highly epitaxial, as deduced by the Gaussian fit of the RC, its FWMH$_{CoO}$ = 0.055(5)$^\circ$ being close to the value obtained from the monocrystalline Si substrate (FWMH$_{Si}$ = 0.040(5)$^\circ$). Moreover, the growth mismatch between the CoO film and the Si substrate was found to originate a tilt of 0.050(5)$^\circ$.

## 4. Conclusions

The growth evolution of cobalt oxides has been studied as a function of $O_2$ pressure in the deposition chamber. The versatility of the PLD technique allowed the variation of this parameter within a wide pressure range (higher with respect to the value currently utilized in other reactive deposition technique) and the identification of the optimum conditions to obtain CoO films with uniform composition. An additional cap-layer was however necessary to avoid further oxidation of the film surface.

The samples showed a homogeneous composition in the whole thickness, a single crystal-like monocrystalline order with high degree of epitaxy and very low roughness. These properties make such samples interesting for both applications and basic research.

## References

[1] M. Gomi, J. Alloys Compd. 326 (2001) 221.
[2] M. Rusop, K. Uma, T. Soga, T. Jimbo, Mater. Sci. Eng. B 127 (2006) 150.
[3] J. Nogués, I.K. Shuller, J. Magn. Magn. Mater. 192 (1999) 203.
[4] T.J. Jackson, S.B. Palmer, J. Phys. D: Appl. Phys. 27 (1994) 1581.
[5] V. Pralong, J.-B. Leriche, B. Beaudoin, E. Naudin, M. Morcrette, J.M. Tarascon, Solid State Ionics 166 (2004) 295.
[6] L. Zbroniec, T. Sasaki, N. Koshizaki, in: Proceedings of the Technical Digest of the 10th International Meeting on Chemical Sensors, Tsukuba, Japan, (2004), pp. 358–359.
[7] R. Caminiti, V. Rossi Albertini, Int. Rev. Phys. Chem. 18 (1999) 263.
[8] R. Felici, F. Cilloco, R. Caminiti, C. Sadun, V. Rossi Albertini, Patent No. RM 93 A000410, Italy, 1993.
[9] E. Agostinelli, S. Kaciulis, M. Vittori-Antisari, Appl. Surf. Sci. 156 (2000) 143.
[10] V.M. Jiménez, J.P. Espinós, A.R. González-Elipe, Surf. Interf. Anal. 26 (1998) 62.
[11] L. Armelao, D. Barreca, S. Gross, A. Martucci, M. Tieto, E. Tondello, J. Non-Cryst. Solids 293–295 (2001) 477.
[12] H.A.E. Hagelin-Weaver, G.B. Hoflund, D.M. Minahan, G.N. Salaita, Appl. Surf. Sci. 235 (2004) 420.
[13] T.J. Chuang, C.R. Brundle, D.W. Rice, Surf. Sci. 59 (1976) 413.
[14] J.S. Pan, E.S. Tok, C.H.A. Huan, R.S. Liu, J.W. Chai, W.J. Ong, K.C. Toh, Surf. Sci. 532–535 (2003) 639.
[15] E. Comini, A. Cusmà, S. Kaciulis, S. Kandasamy, G. Padeletti, L. Pandolci, G. Sberveglieri, A. Trinchi, W. Wlodarski, Surf. Interf. Anal. 38 (2006) 736.